Computer Vision and Image Understanding 165 (2017) 33–42

Contents lists available at ScienceDirect

Computer Vision and Image Understanding

journal homepage: www.elsevier.com/locate/cviu

Atmospheric light estimation in hazy images based on color-plane model

Ming-Zhu Zhu[a,b], Bing-Wei He[*,a,b], Li-Wei Zhang[a,b]

[a] College of mechanical design and manufacture, Fuzhou University, Fuzhou, China
[b] Collaborative innovation Center of High-End Manufacturing Equipment of FuJian Province, Fuzhou, FuJian, China

ARTICLE INFO

Keywords:
Dehaze
Single image
Air light estimation
Model

ABSTRACT

In this paper, a novel air light recovery method based on color-plane model is proposed. The method aims to improve the robustness of air light estimation for single image dehazing applications. Traditional methods estimating air light rely on user input or dense haze region. It is unstable when dense haze region is not included. The methods based on the color-line model and haze-line model achieve significant improvements on air light estimation without identifying dense haze regions. However, both of the models are lack of generality. Therefore, we propose the color-plane model which combines the color-line model and haze-line model. It is motivated by the fact that colors with a common direction widely exist and tend to stay together in natural images. These colors spread on color-plane after being blended with haze, which indicates the orientation of the air light. An algorithm based on region growing is designed to extract potential color-plane in haze images. RANSAC is employed to estimate the air light orientation. The magnitude is estimated based on the assumption that the intensities of several bright pixels in different depth ranges should be similar. A novel algorithm based on energy minimization is proposed to estimate depth ranges. Experimental results show that the proposed method performs better than state-of-the-art methods.

1. Introduction

Hazy scenes widely exist in the outdoor environment, which generally have limited visibility and low contrast. Image dehazing is highly important to both photography application and computer vision application. For photography applications, it corrects the brightness and color shift of haze images and makes them more visually pleasuring. For computer vision, it can generate the approximation of the scene radiance map, which is usually the input of most image analysis or object recognition algorithms.

The goal of haze remove is to recover the RGB values of the haze-free image. It is still an open problem. The legend methods need additional information such as: scene geometry model (Kopf et al., 2008), multi-images of a same scene under different weather conditions (Narasimhan and Nayar, 2000) or different degrees of polarization state (Schechner et al., 2001). The constraint of such additional input limits these methods.

As a contrast, single image dehazing attracts more attentions. There are two categories of approaches: enhancement based methods and physical methods. Enhancement based methods aim to emphasize specific properties of haze images. As examples, Tan (2008) solves haze-free images by maximizing the contrast of each small patch. Bekaert et al. (2012) and Ancuti and Ancuti (2013) proposed fusion-based methods that fuse the results of white balance, contrast enhancement and so on. Choi et al. (2015) proposed a non-reference perceptual fog density prediction model and enhance haze images based on this model. The results of these methods are commonly of high contrast but lack of physical interpretation. Physical methods usually interpret the haze image as a blending of the haze-free image and the atmospheric color. Transmission map and air light (atmospheric light) estimations are the two major parts in these approaches. Various assumptions, priors or models were proposed for transmission map estimation, such as: color features (Park et al., 2013; Li and Zheng, 2015; Zhu et al., 2015), independent assumptions (Fattal, 2008; Nishino et al., 2012), the dark channel prior (He et al., 2010), the color-line model (Fattal, 2014), the haze-line model (Berman et al., 2016), patch recurrence model (Bahat and Irani, 2016) etc. A related work proposed by (Tang et al., 2014) examines various priors in a learning framework. A comprehensive survey of dehazing algorithms is published in Li et al. (2016).

Air light estimation was not been studied extensively as transmission map estimation. However, its performance affects the quality of haze removal results even more significantly. As shown in Fig. 1, given a common transmission map, errors on air light cause color shift and incorrect brightness globally. In addition, most dehazing methods require a known air light to estimate transmission map.

* Corresponding author.
E-mail addresses: lilinfzu@163.com (M.-Z. Zhu), mebwhe@fzu.edu.cn (B.-W. He), lw.zhang@fzu.edu.cn (L.-W. Zhang).

http://dx.doi.org/10.1016/j.cviu.2017.09.005
Received 17 December 2016; Received in revised form 5 June 2017; Accepted 27 September 2017
Available online 11 October 2017

Fig. 1. Haze removal results with given transmission map and different air lights. a) proper air light. b) air light with wrong orientation. c) air light with small magnitude. d) air light with large magnitude.

In early works, the brightest pixel was used to estimate the air light. Tan (2008) chose the brightest pixel and Fattal (2008) used it as an initial guess. However, in practice, the brightest pixel may correspond to a bright object rather than the air light. To tackle this problem, He et al. (2010) pick the brightest pixel among the pixels that have the top brightest values of the dark channel. Cai et al. (2016) estimate the transmission map first and then select the brightest pixel whose transmission value is smaller than 0.1. These methods require a visible area with no objects in line-of-sight. These methods are not robust when the condition is not satisfied.

Tarel and Hautire (2010) apply white balance on the haze image and assume the air light is pure white. Meng et al. (2013) estimate each channel of the air light individually. The maximum value of each channel is taken as the estimate of the component of the air light. It is the same as performing a max-RGB white balance on the haze image, which is more robust but still error-prone.

Sulami et al. (2014) estimate the air light magnitude and orientation respectively. The orientation estimation is based on the color-line model proposed by Fattal (2014). It first selects small patches with a constant transmission and surface albedo. The colors in each patch are assumed to follow the color-line model. These colors form a line crossing the air light in RGB-space, namely color-line. The optimal orientation is the vector that crosses most of color-line. The magnitude is recovered by minimizing the dependence between the brightest pixels and their transmission values. The method ignores the existence of line distribution colors that do not follow the color-line model. It may cause extreme failure in some cases.

The patch recurrence property is an observation that small image patches tend to repeat inside a single natural image, both within the same scale and across different scales. Based on this prior, Bahat and Irani (2016) detect difference between such co-occurring patches and calculate the air light. The method is computationally intensive and the assumption is relatively weak.

Pixels with same color but different depth widely exist in natural images. After blending with haze, the colors of these pixels form a line pointing to the air light in RGB space. These lines are modeled as haze-lines by Berman et al. (2016). Based on this model, Berman et al. (2017) use Hough transform in RGB space to find the location of the air light. The method is computationally efficient but lacks of accuracy when the model is not valid, such as a landscape with distinct colors in different depth ranges. Furthermore, the method prefers the air light close to pixel colors. It implicitly relies on haze intensity regions.

In this paper, we propose the color-plane model which integrates the color-line model and the haze-line model. Pixels satisfying the model are found by a brief scanning and region growing algorithm. The model can fit a large number of pixels in a haze image, which benefits the outliers exclusion ignored by the color-line model. The proposed method is also suitable to the scene contains distinct colors in different depth ranges, to which the haze-line model is not suitable. The orientation of the air light is estimated based on RANSAC. The magnitude is estimated based on the assumption that the intensities of several bright pixels in different depth ranges should be similar.

The remainder of this paper is organized as follows: Section 2.1 introduces the physical model of haze images. Section 2.2 introduces the color-line model and haze-line model. The color-plane model is proposed in Section 2.3. The prior of color-plane extraction is tested in Section 3. Sections 4.1 and 4.2 introduce the method of air light orientation estimation. Section 4.3 introduces the method of depth range estimation. Section 4.4 introduces the method of air light magnitude estimation. Section 5 introduces experiments on synthetic and natural images. Conclusions are given in Section 6.

2. Background

2.1. Haze model

The physical model widely used to describe the formation of a haze image is as follows (Middleton, 1954):

$$I(x) = t(x)J(x) + (1 - t(x))A. \tag{1}$$

where x is the pixel coordinate, $I(x)$ is the observed image, $J(x)$ is the scene radiance. T is the transmission map which describes the portion of the light reflected by the scene and finally reaches the camera. It only depends on the scene depth when the haze is uniformly distributed. A is the air light, the color we aimed to estimate.

2.2. Color-line and haze-line

Natural environments are typically composed of distinct objects. Each has its own surface reflectance properties. Based on this fact, Fattal (2014) proposed the color-line model used for image dehazing. Sulami et al. (2014) followed this model and proposed an air light estimation method. Berman et al. (2016) proposed the haze-line model based on the fact that the color distribution of natural images is sparse. An air light estimation method (Berman et al., 2017) was proposed based on this model.

The color-line model and haze-line model can be integrated together by following the model

$$J(x) = l(x)R(x), \tag{2}$$

where, $R(x)$ is the relative intensity of each channel of the reflected light, namely $\|R(x)\| = 1$. $l(x)$ is the magnitude of the radiance. R corresponds to the surface reflectance or albedo and l to the incident light or shading. Based on this, Eq. (1) becomes

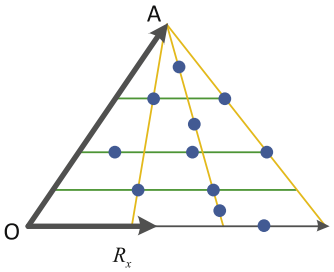

Fig. 2. The color-line model and haze-line model. The colors with same albedo R_x are blended with the air light A, shifted along the yellow lines, namely haze-line. In a small patch, colors are blended with A by similar ratios, formed one of the green lines, namely color-line. (For interpretation of the references to colour in this figure legend, the reader is referred to the web version of this article.)

$$I(x) = t(x)l(x)R(x) + (1 - t(x))A. \tag{3}$$

The color-line model assumes that $t(x)$ and $R(x)$ are constant in a small image patch. It means

$$I(y) = l(y)t_x R_x + (1 - t_x)A, \quad y = \Omega(x), \tag{4}$$

where $\Omega(x)$ is a small patch centered at pixel x. t_x and R_x are constant in the patch. The collection of $I(y)$ forms a line in RGB-space with direction $t_x R_x$ and offset $(1 - t_x)A$, namely color-line.

Since the color distribution of natural images is sparse. The haze-line model collects these colors in haze images. It becomes

$$I(y) = t(y)l_x R_x + (1 - t(y))A, \quad y = \{y | l(y)R(y) = l_x R_x, y \in I\}. \tag{5}$$

The collection of $I(y)$ forms a line with two endpoints located at $l_x R_x$ and A, namely haze-line.

Fig. 2 shows an example of color-line and haze-line. In a haze-free image, colors with same direction R_x are scattered on the vector R_x. While misting, each color is blended with the air light A, shifted along the yellow lines. This is the phenomenon described by the haze-line model. In a small patch, colors are blended with A by similar ratios, forming a line paralleling with R_x. This phenomenon is described by the color-line model, shown as green lines.

The color-line model and haze-line model are valuable to air light estimation. It is obviously that a good air light should intersect color-line, or be the intersection point of many haze-line.

2.3. Color-plane model

In practice, many lines can be fitted in $I(x)$, but only a small portion of the lines follow the color-line model or the haze-line model. Fattal (2014) and Sulami et al. (2014) checked every image patch to extract color-line. The local constant assumption of scene albedo and transmission limits the size of the patch, which affects the accuracy of linear fitting. The haze-line model also contains an assumption on transmission. If colors in each cluster spread on similar transmission ranges, haze-lines are quite short. It affects the accuracy of subsequent algorithms. It happens in the example shown in Fig. 3. Pixels of closed scenes are mainly yellow and slightly similar colors exist in distant scenes. The haze-lines formed by these pixels are short while the color-lines are not affected.

Refering to Fig. 2, it is obvious that the color-line and the haze-line are complementary. They actually form a plane expanded by A and R_x in RGB-space. Pixels in each plane have the same albedo in haze free image. Therefore, we propose the color-plane model which combines the two models. The pixels forms a color-plane if

$$I(y) = t(y)l(y)R_x + (1 - t(y))A, \quad y = \{y | R(y) = R_x, y \in I\}. \tag{6}$$

Note that there is no constraint on transmission. The color-plane model is also valuable to air light estimation. A good air light should perpendicular to the normal vector of each color-plane.

3. The prior

Given a number of pixels, the color-plane model is satisfied if the color-line model or the haze-line model is satisfied. The feasibility of identifying color-line was illustrated by Fattal (2014) and Sulami et al. (2014). The existence of haze-line was proved by Berman et al. (2016). Based on these previous works, we further test four probabilities p_1, p_2, q_1, q_2. Given a random patch of haze-free image, p_1 is the probability of that the pixels inside form a line, and p_2 is the condition probability of that the pixels have a common orientation (forming a line crossing the origin). When p_1 happens, we further check the number of the adjacent pixels that follow the fitted line. The number is sufficient when it is bigger than a thousandth of the pixels number. q_1 is the probability that the number is sufficient when $p_1(1 - p_2)$ happens. q_2 is the probability that the number is sufficient when $p_1 p_2$ happens.

Haze free images are provided by the BSD500 (Berkeley Segmentation Dataset (Martin et al., 2001)) and the WED (Waterloo Exploration Database (Ma et al., 2016)). Since haze usually occurs in outdoor landscape and cityscape scenes, we manually pick out 500 images of each type.

The images of BSDS500 have the same number of pixels (481 * 321 or 321 * 481) while the images of WED have not. We resize these images to common size. For each sample, we check every patch of 5×5 pixels and employ the PCA (principle component analysis) on the colors in RGB-space. A line is found if $\lambda_1 > 1000\lambda_2$, where λ_1 is the principal component and λ_2 is the secondary component. If the line is longer than 0.3 (colors range from 0 to 1), it is valid and counted in p_1. If the distance from the origin to the line is less than 0.05, the line is counted both in p_1 and p_2. For region growing, a pixel is annexed to the region if the block distance is less than 3.

Results show that, for outdoor landscape, p_1 is 0.61% and p_2 is 27%, q_1 is 42% and q_2 is 58%. It means that, for outdoor landscape, we can find averagely 942 patches (if the image have the same size as the images of BSDS500) that the colors inside form a line in RGB-space. Furthermore, if we only consider the patches that can be extended enough, approximate 34% of the patches follow the color-plane model. For cityscape, p_1 is 2.4% and p_2 is 39%, q_1 is 47% and q_2 is 61%. The final probability of being a color-plane is 74%. These is because of the wide existence of diffuse surfaces in cityscape images.

Fig. 3 shows an example of color-plane. Fig. 3a is a haze free image. Two groups of pixels that have similar orientations are marked as green and blue. The colors are displayed in Fig. 3c. They form two lines cross the origin. Synthetic haze is added in Fig. 3b. The same pixels are displayed in Fig. 3d. The pixels marked by blue scatter in the same depth. They have similar transmissions and form a short line shifting toward A. The pixels marked by green scatter in a large range of depth. They have different transmissions so they shift with different degrees and spread on a color-plane. Note that neither the color-line model nor the haze-line model is able to fit such pixels. Fig. 3e shows this distribution in another view. It shows that the normal vector of the color-plane is perpendicular to the air light A.

The prior indicates a frame to extract color-planes: In haze images, we search patches that the colors spreading on a plane cross the origin (colors can spread as a line or a plane). Approximately, an average of 27% of the extracted planes are color-plane for outdoor landscape and 39% for cityscape. Furthermore, if we apply region growing and filter out the patches can not be extended sufficiently. An average of 34% of the extracted planes are color-plane for outdoor landscape and 74% for cityscape.

4. New approach

Our method is consist of 4 steps: a) Extract pixels that support color-plane model based on region growing. b) Estimate the air light orientation based on RANSAC. c) Estimate the depth label map that

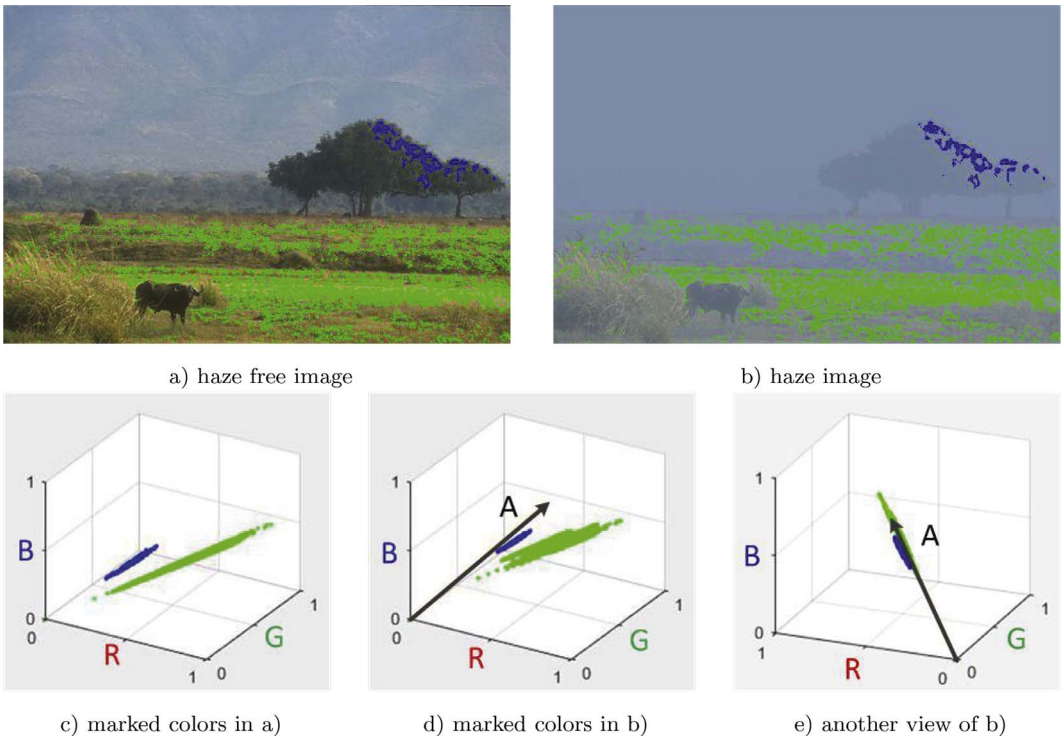

Fig. 3. a) Haze free image with two clusters of pixels marked by green and blue. The colors within have the same orientation. b) Synthetic haze image. c) The marked colors in RGB-space. d) The marked colors in RGB-space after blending with haze. e) Another view of d). (For interpretation of the references to colour in this figure legend, the reader is referred to the web version of this article.)

segments the haze image into several depth ranges. d) Estimate the air light magnitude based on a global brightness assumption.

4.1. Extracting regions that follow color-plane model

Region growing is applied to extract color-plane. To find seed regions, every patch (5×5 in this case) is checked to see whether the colors spread on a plane. A patch contains m colors is expressed as a matrix P contains $m \times 3$ elements. Since desired planes must cross the origin, we do not use the PCA directly. Instead, the covariance matrix of $P'P$ is calculated. The eigenvectors v and the eigenvalues λ of the covariance matrix are solved. A new coordinate frame is constructed based on P, v and λ. The origin is the center of P. The major vector v_1 is taken as the x-axis of the plane and the least weighted vector v_3 is taken as the z-axis of the plane. If the z-value of each color is less than 0.003 and the maximum x-value is bigger than 0.2 (color distribution is tighter after blending with haze, therefore the threshold used here is smaller than the one used in the prior), the patch is included as a seed region.

Given a seed region, the algorithm keeps checking adjacent pixels. If a pixel follows the current plane (z-value is less than 0.003), the region grows by including it. The region keeps growing until there is no more supporting pixels or the area is bigger than a threshold (40 times of the patch size). If the growth stops with enough size (a thousandth of the image size), the normal vector of the fitted plane is recorded and the pixels inside are removed from the image.

There is a high probability that scene albedos across an edge are different. Therefore, we extracted image edges on hue map in HSV-space by canny method. The growing process is not allowed to start or stride over these edges.

4.2. Estimating the air light orientation

Based on the definition in Eq. (6), the air light is perpendicular to every normal vector of color-plane. Theoretically, the orientation of air light A_e can be solved by $A_e = n_1 \times n_2$ where n_1 and n_2 is a random pair of normal vectors. However, as shown in the prior, averagely, 34% of the extracted planes are real color-plane for landscape images and 74% for cityscape images. To avoid the effect of these false data, we employ RANSAC framework to solve the optimal A_e.

In each loop of RANSAC, a pair of normal vectors is picked randomly. A temporary air light orientation $\widehat{A}_e$ is solved and evaluated by

$$\sum_{i \in N} w_i \{[90 - ang(\widehat{A}_e, n_i)] < 0.1\}, \tag{7}$$

where $ang(\widehat{A}_e, n_i)$ is the angle between $\widehat{A}_e$ and n_i. N is the set of the normal vectors of extracted planes. w_i is the weight of ith plane which is proportional to the number of pixels within, and $\sum_{i \in N} w_i = 1$. The loop stops while $\widehat{A}_e$ scores over 0.5 or the maximum iterations 1000 is reached. The supporters of the optimal $\widehat{A}_e$ are used to calculate A_e through the least square method.

Fig. 4 shows an example of planes extraction and air light orientation estimation. Colors in each frame spread on a color-plane in RGB-space. The normal vectors of these three planes are displayed in Fig. 4b. The true air light is perpendicular to these vectors.

4.3. Estimating the depth label map

The color-plane model does not impose any restriction on the air light magnitude. To solve the magnitude, we follow the assumption proposed by Sulami et al. (2014). It assumes that the intensities of several brightest pixels (top 10% in this case) in different depth ranges should be equal. The assumption implies that the haze removal result or at least a depth map is required. Sulami et al. (2014) rely on other dehazing methods to offer the haze removal result, which is inconvenient. In this paper, we propose a novel algorithm to offer the rough depth map.

Since the intervals of different depth ranges is unnecessary to be exactly the same, the inverse-transmission map $s = 1 - t$ can be used. Therefore, the assumption is

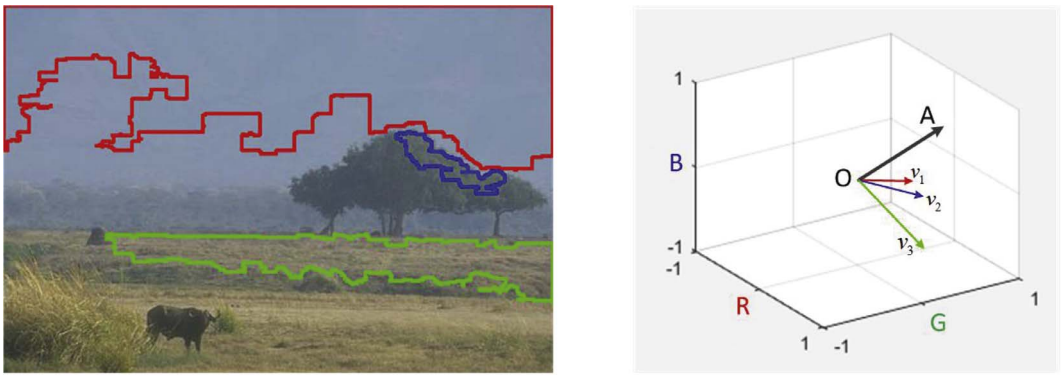

a) haze free image and color-plane b) normal vectors of color-plane

Fig. 4. An example of color-plane in haze image. a) haze image and three frames. Colors in each frame scattered on a color-plane in RGB-space. b) the true air light and the normal vectors of the planes.

$$\overline{J}_n = avermax\{J^g(x)|\tilde{s}(x) = n\} \equiv k, \tag{8}$$

where $J^g(x)$ is the intensity of $J(x)$, $\tilde{s} = round\{Ns(x)\}$ is the depth label map, *avermax* means the average intensity of the top 10% bright pixels.

The depth map s can be solved by seeking a configuration which minimizes the energy function

$$E(s) = \sum_x D(x) + \sum_{\{x,y\}\in N} K(x, y), \tag{9}$$

where $D(x)$ is the bound term, $K(x, y)$ is the smoothness term. The smoothness term introduces the piece-wise smooth property. It means that, for adjacent pixels, the depth values should be similar if their colors are similar. It is defined as

$$K(x, y) = \frac{[s(x) - s(y)]^2}{\|I(x) - I(y)\|_2^2}. \tag{10}$$

The bound term is to judge whether a depth value is valid. There is no penalty if the value is valid. It is

$$D(x) = \begin{cases} 0 & s(x) \in L(x) \\ \infty & s(x) \notin L(x). \end{cases} \tag{11}$$

where $L(x)$ is the label set contains all valid $s(x)$. The definition of the label set is

$$L(x) = \{s_{UB}(y)|y \in \Omega(x), s_{UB}(y) < s_{UB}(x)\}, \tag{12}$$

where s_{UB} is the upper-bound of the depth map,

$$s_{UB} = \frac{1}{\eta}\min_c \frac{I^c}{A_e^c}. \tag{13}$$

It is derived from Eq. (1) based on the fact that the scene radiance is nonnegative. The label set is defined based on the following assumption: In a small patch of haze image centered at x, at least one pixel $y \in \Omega(x)$ satisfies $\min_{c\in\{r,g,b\}} J^c(y) = 0$ and $t(x) = t(y)$. The first equation is known as the dark channel prior (He et al., 2010). The second equation is more general than the local constant assumption which is widely used (Bahat and Irani, 2016; Fattal, 2014; He et al., 2010).

The minimization of Eq. (9) is a multi-label problem. We solved the problem via α-expansion algorithm (Boykov and Kolmogorov, 2004; Boykov et al., 2001; Kolmogorov and Zabih, 2004). It is time consuming since there are hundreds of labels. Fortunately, we only need a rough segmentation of the depth. Therefore, the right side of Eq. (13) was scaled and rounded. Furthermore, the magnitude η is replaced by a selected $\eta_{\min}$ (0.5 in this case). It becomes

$$\tilde{s}_{UB} = round\left\{\frac{N}{\eta_{\min}}\min_c \frac{I^c}{A_e^c}\right\}. \tag{14}$$

Finally, a configuration $\tilde{s}$ is solved and the depth map is approximated as

$$s = \alpha\tilde{s} = \frac{\eta_{\min}}{N\eta}\tilde{s}. \tag{15}$$

Fig. 5 compares the proposed algorithm with the method of He et al. (2010) and Berman et al. (2016). As shown, the result of He et al. (2010) contains lots of improper details whereas the result of Berman et al. (2016) contains over-smoothness edges. The proposed algorithm offers the best depth label map which meets the requirements.

4.4. Estimating the air light magnitude

The intensity in Eq. (1) is

$$I^g(x) = t(x)J^g(x) + [1 - t(x)]\eta A_e^g, \tag{16}$$

where A_e^g is the intensity of A_e. Since we only need a rough intensity estimation of each depth range, the equation can be approximated as

$$I^g(x) = [1 - s(x)]J^g(x) + s(x)\eta A_e^g. \tag{17}$$

The average intensity of bright pixels in each depth range becomes

$$\overline{J}_n = \frac{Q_n}{1 - \alpha n}, \tag{18}$$

where Q_n is only related to n as

$$Q_n = \overline{I}_n - \frac{n}{N}\eta_{\min} A_e^g, \quad \overline{I}_n = avermax\{I^g(x)|\tilde{s}(x) = n\}. \tag{19}$$

Considering the assumption in Eq. (8), the average intensity k and the scale α in Eq. (15) can be solved by minimizing

$$E(\alpha, k) = \sum_n \left(\alpha n + \frac{1}{k}Q_n - 1\right)^2. \tag{20}$$

It can be solved by the least square method with the standard form

$$\begin{bmatrix} 0 & 1 & 2 & \cdots & N \\ Q_0 & Q_1 & Q_2 & \cdots & Q_N \end{bmatrix}^T \begin{bmatrix} \alpha \\ 1/k \end{bmatrix} = [1 \;\; 1 \;\; 1 \;\; \cdots \;\; 1]^T. \tag{21}$$

Given α, η can be solved based on Eq. (15).

With certain algebraic operations, it can be shown that $\eta = \overline{I}_n/A_e^g$ satisfies the last column of Eq. (21). It is consistent with the intuition that bright pixels at large distance reflects the air light, which is widely used in traditional methods (He et al., 2010; Tan, 2008). However, we neither assume the existence of large distance regions nor heavily rely on them. Instead, the magnitude is estimated by considering all depth ranges.

Fig. 5c shows an example. The low magnitude (η=1.00) leads to an over-bright result whereas the high magnitude (η = 1.36) leads to a

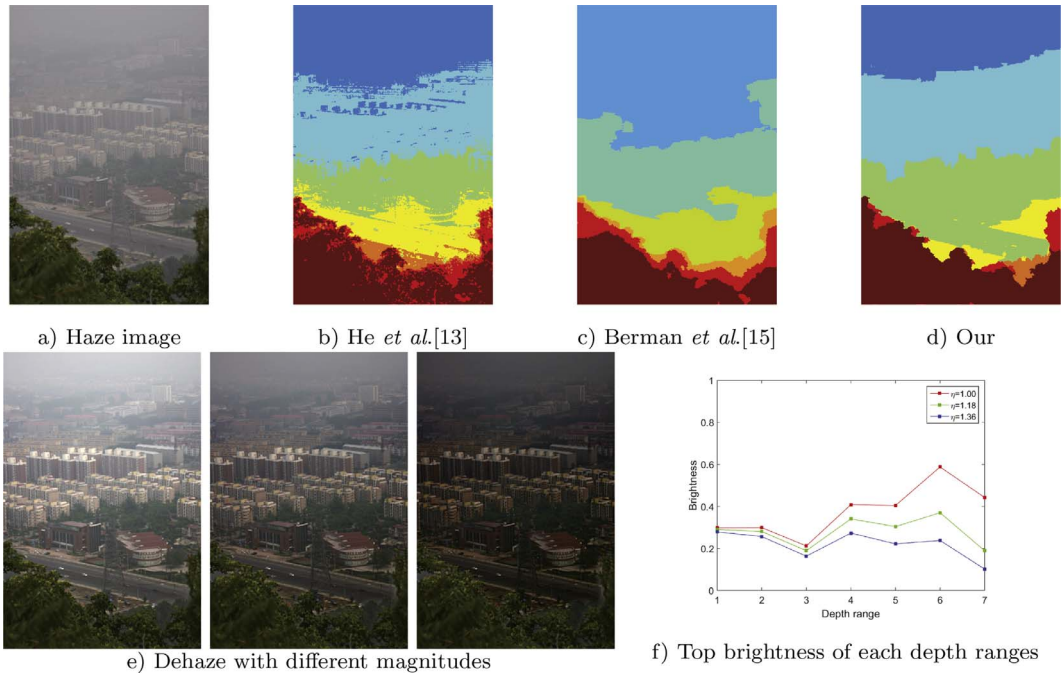

Fig. 5. a) haze image. b) depth label map provided by He et al. (2010). c) depth label map provided by Berman et al. (2016). d) depth label map provided by our method. e) haze removal results of different magnitudes. From left to right: $\eta = 1.00, 1.18, 1.36$. f) the average intensities of top 10% pixels in different depth ranges.

gloomy result. Fig. 5f shows that pixels at larger distance change more significantly. The proper magnitude ($\eta = 1.18$) which minimize the Eq. (20) gives the optimal result.

5. Experiment

The proposed method was compared with the methods He et al. (2010), Bahat and Irani (2016), Sulami et al. (2014) and Berman et al. (2017). We evaluate these methods by: 1)assessing the accuracy of air light estimation on synthetic images with known truth. 2)assessing the accuracy on natural images with manual selected truth. 3)comparing the performance of the proposed methods against the existing methods.

5.1. Synthetic images

The D-HAZY dataset (Ancuti et al., 2016) provides synthetic haze images by blending haze free images and pure white air light. It was built based on the Middelbury and NYU Depth datasets. It also provides corresponding haze-free images and transmission maps. Based on these data, we extended the dataset by reproducing haze images. For each sample, 5 haze images were produced with random air lights. Each element of the air light was sampled in the range [0.7, 1]. Only the part of Middelbury dataset was used due to its high quality. Finally, there are 115 haze images tested.

The orientation and magnitude errors are reported in Tabel 1. Our method produces the best performance on orientation estimation. It is also competitive on other aspects. Fig. 6 shows two examples of synthetic images and our results.

5.2. Natural images

For natural images, sky regions are selected and used as ground-truth. We selected haze images with uniform sky region from the FADE dataset (Choi et al., 2015). However, manual selection is exhausting and lacks of accuracy. Therefore, the qualitative comparison is carried out in this experiment. 6 examples of different types are displayed in Fig. 7. Orientation errors below 0.5 (degree) and magnitude error below 0.05 are marked as blue.

Table 1
Comparison on synthetic images. Air light estimation method includes: He et al. (2010), Bahat and Irani (2016), Sulami et al. (2014), Berman et al. (2017) and our method.

	Orientation		Magnitude	
	Mean	Median	Mean	Median
He	0.438	0.393	0.073	0.085
Bahat	0.671	0.620	0.121	0.130
Sulami	0.532	0.540	0.063	0.062
Berman	0.465	0.435	**0.056**	**0.052**
Our	**0.409**	**0.385**	0.061	0.063

As shown, the method proposed by He et al. (2010) performs the best. It is conceivable because the method is consistent with the intuition of manual selection. When the uniform sky region is adopted, the high quality of the processing results is anticipated. However, in practice, there is a large number of haze images without sky region. Furthermore, sky regions are unnecessary to be uniform. Instead, it can be colorful or over-bright.

For the light haze image in Fig. 7, the haze-line model is barely supported. Therefore, the method proposed by Berman et al. (2017) does not perform well. The color-line model is supported by several haze pixels in far distance. The orientation results of Sulami et al. (2014) and ours are good. However, our method fails to estimate the magnitude. It is probably because the depth range is not well estimated. For the thick haze image, the color-line and haze-line models are well supported. However, the image colors are monotonic, which makes the normal vectors of color-plane stay close. It reduces the accuracy of our method. For the landscape and cityscape, our method performs well. Most of haze images are one of these kinds. The gloom image is very challenging. Only He et al. (2010) performs well. From highlighted images, it also shows the promising performance of the proposed method.

As mentioned above, a number of haze images do not contain sky region. To evaluate the performance of each method in this case, we cropped the selected regions on the samples. Results are shown in Fig. 8, only the cropped regions were taken as the input images. As

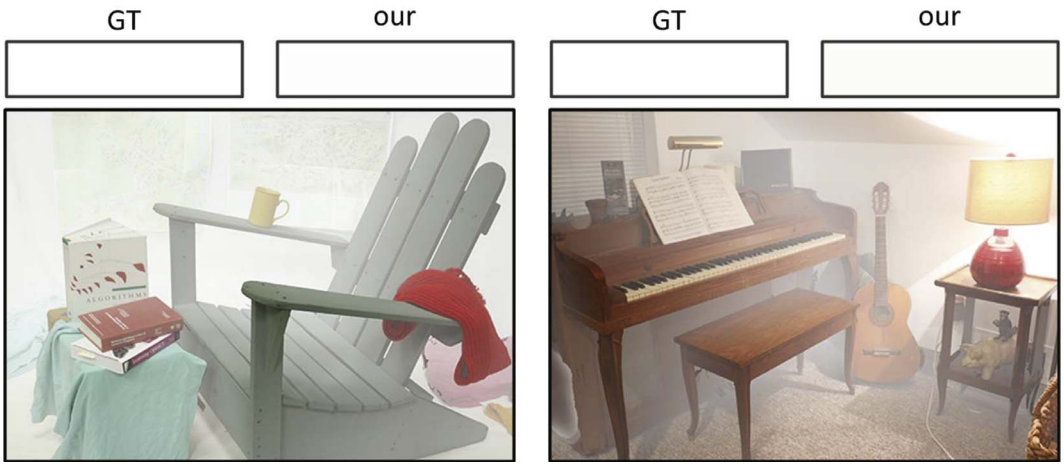

Fig. 6. Two of the synthetic images tested. The ground truths and our results are displayed.

shown in the images, the method proposed by He et al. (2010) fails in this case. For landscape, cityscape and highlighted image, our method is more robust. It obtains good results on orientation estimation.

In summary, our method shows a robust performance on landscape and cityscape, although, it does not perform well on severely light haze or thick haze. The orientation estimation is nearly independent from the existence of sky region. The magnitude estimation is acceptable in most cases.

5.3. Comparison experiments

A comparison experiment is carried out to evaluate the performance improvements on air light estimation. Three typical and available dehazing methods proposed by He et al. (2010), Meng et al. (2013) and Berman et al. (2016) are used. Each pair of air light estimation method and dehazing method are tested on both synthetic and natural images.

Synthetic images are provided by the D-HAZY dataset (Ancuti et al.,

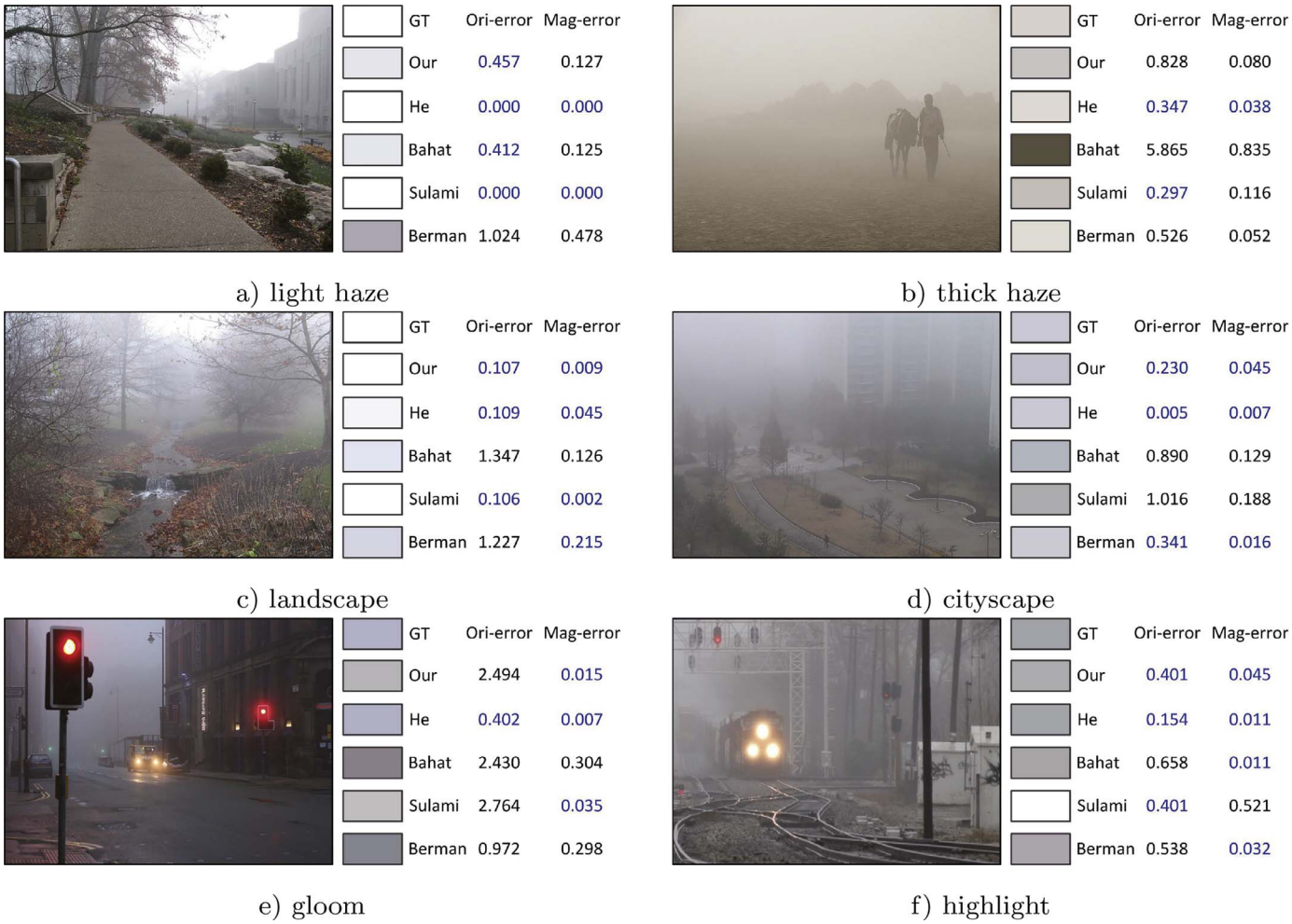

Fig. 7. Comparison on natural images. Air light estimation methods include: He et al. (2010), Bahat and Irani (2016), Sulami et al. (2014), Berman et al. (2017) and our method. Ground truths were selected manually from sky regions.

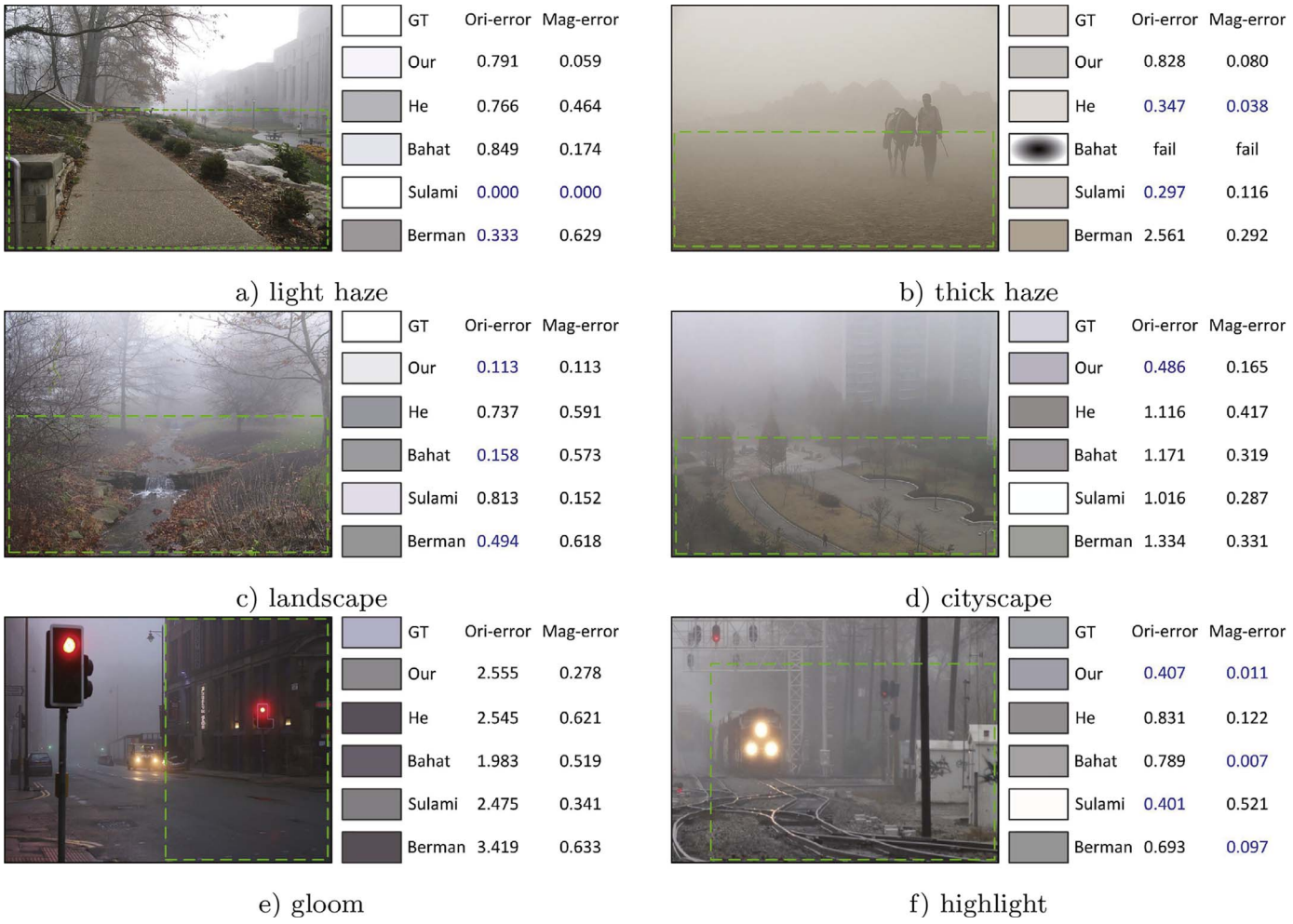

Fig. 8. Comparison on natural images without sky region. Only the framed sections were taken as the input images.

Table 2
Evaluation of each pair of air light esimation and dehazing methods on synthetic images. Air light estimation methods displayed in the top are: He et al. (2010), Bahat and Irani (2016), Sulami et al. (2014), Berman et al. (2017) and our method. Dehazing methods displayed in the left are: He et al. (2010), Meng et al. (2013) and Berman et al. (2016).

		He	Bahat	Sulami	Berman	Our
He	SSIM	0.734	0.727	0.736	0.736	**0.738**
	PCQI	0.805	0.784	0.791	0.845	**0.861**
Meng	SSIM	0.546	0.573	0.583	**0.591**	0.590
	PCQI	0.712	0.739	0.741	0.797	**0.802**
Berman	SSIM	0.651	0.703	0.645	**0.712**	0.691
	PCQI	0.901	0.921	0.907	**0.924**	0.923

Table 3
Evaluation of each pair of air light esimation and dehazing methods on natural images. Air light estimation methods displayed in the top are: He et al. (2010), Bahat and Irani (2016), Sulami et al. (2014), Berman et al. (2017) and our method. Dehazing methods displayed in the left are: He et al. (2010), Meng et al. (2013) and Berman et al. (2016).

		He	Bahat	Sulami	Berman	Our
He	FADE	1.161	1.119	1.150	1.166	**1.205**
	NR-CD	1.205	1.118	1.160	1.202	**1.261**
Meng	FADE	1.217	1.126	1.021	1.225	**1.227**
	NR-CD	1.237	1.205	0.882	1.318	**1.335**
Berman	FADE	1.231	1.110	1.031	**1.256**	1.232
	NR-CD	0.977	0.939	0.898	**0.984**	0.951

2016). Only the images provided by Middelbury dataset was used because of its high quality. The SSIM (structural similarity index) (Wang et al., 2004) was used to evaluate the quality of haze removal results. The PCQI (patch-based contrast quality index) proposed by Wang et al. (2015) is used to measure the contrast variations between haze removal results and ground truths. The results are shown in Tabel 2.

Natural haze images are provided by the FADE dataset (Choi et al., 2015). The FADE (fog aware density evaluator) index associate with the dataset was also used to evaluate the haze amount of haze removal results. To evaluate the quality of contrast, we employed the NR-CD (no-reference contrast-distort index) proposed by Fang et al. (2015). For each sample, FADE and NR-CD are measured before and after haze remove. The difference of each index indicates the improvement. The average improvements are shown in Tabel 3.

As shown in the table, the proposed method performs much better than He et al. (2010) and Meng et al. (2013). The method of Berman et al. (2016) also performs well. Fig. 9 shows examples of synthetic images. From the first image, the improvement can be seen on the cardboard. For the second image, colors of the curtain of the proposed method is more closed to the ground truth. For the third image, the tone of our result is obviously better.

Fig. 10 shows the processing results of the natural images. From the first image, the improvement can be seen on the pillars and the branches beside the hollow. The pillars provided by He et al. (2010) is overbright and the branches are hard to see. By employing the air light estimate of the proposed method, these problems are eliminated. From the last two images, the results of Meng et al. (2013) and

Fig. 9. An example of the improvement introduced by our method. a,e,i) synthetic haze images. b,f,j) haze removal results of He et al. (2010), Meng et al. (2013) and Berman et al. (2016). c,g,k) haze removal results with the air light estimated by our method. d,h,l) the ground truths.

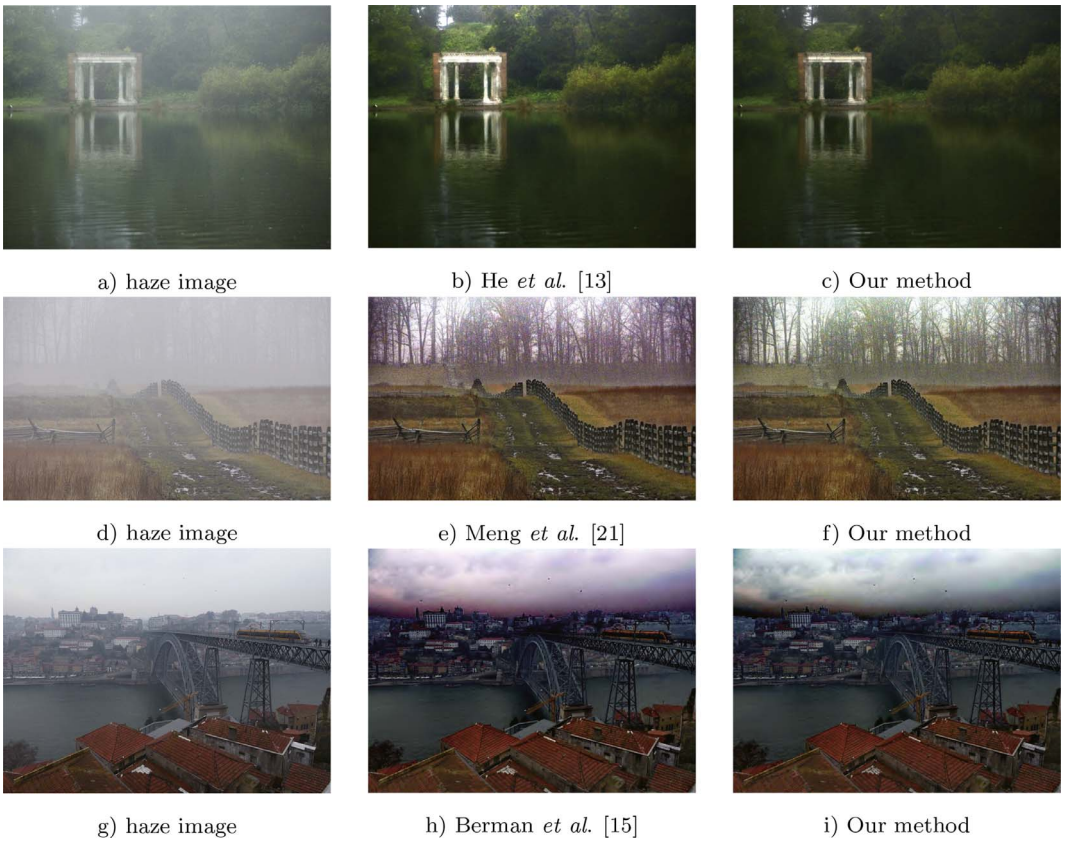

Fig. 10. An example of the improvement introduced by our method. a,d,g) natural haze image. b,e,h) haze removal results of He et al. (2010), Meng et al. (2013) and Berman et al. (2016). c,f,i) haze removal results with the air lights estimates of our method.

Berman et al. (2016) are reddish. The results appear more natural while using the proposed method.

6. Conclusion

We propose a novel air light recovery method with a model named color-plane. The model integrates the color-line model and the haze-line model. It is based on the fact that colors with a common direction are widely exist and tend to stay together in natural images. An algorithm based on region growing and RANSAC was designed for air light orientation estimation. The magnitude is estimated based on the assumption that the intensities of several bright pixels in different depth ranges should be similar. A novel algorithm based on energy minimization is proposed to provide the depth range map.

The method was evaluated on different datasets including synthetic images and natural images. Results show the promising performance on air light orientation estimation, which is critical to ensure faithful colors in haze removal result. Furthermore, the orientation estimation is robust when the sky region is not exist. The magnitude estimation is also competitive. The comparison experiments show that the proposed method can improve haze removal results by providing more accurate air lights.

Acknowledgment

This work was supported by the National Natural Science Foundation of China (Project No. 61473090 and No.61673115) and Fujian Provincial Collaborative Innovation Center for High-End Equipment Manufacturing.

References

Ancuti, C., Ancuti, C.O., Vleeschouwer, C.D., 2016. D-hazy: a dataset to evaluate quantitatively dehazing algorithms. Proc. ICIP. pp. 2226–2230.
Ancuti, C.O., Ancuti, C., 2013. Single image dehazing by multi-scale fusion. IEEE Trans. Image Process. 22 (8), 3271–3282.
Bahat, Y., Irani, M., 2016. Blind dehazing using internal patch recurrence. Proc. ICCP. pp. 1–9.
Bekaert, P., Haber, T., Ancuti, C.O., Ancuti, C., 2012. Enhancing underwater images and videos by fusion. Proc. CVPR. pp. 81–88.
Berman, D., Treibitz, T., Avidan, S., 2016. Non-local image dehazing. Proc. CVPR. pp. 1674–1682.
Berman, D., Treibitz, T., A. S., 2017. Air-light estimation using haze-lines. ICCP.
Boykov, Y., Kolmogorov, V., 2004. An experimental comparison of min-cut/max-flow algorithms for energy minimization in vision. IEEE Trans. Pattern Anal. Mach. Intell. 26 (9), 1124–1137.
Boykov, Y., Veksler, O., Zabih, R., 2001. Fast approximate energy minimization via graph cuts. IEEE Trans. Pattern Anal. Mach. Intell. 23 (1), 1222–1239.
Cai, B., Xu, X., Jia, K., Qing, C., Tao, D., 2016. Dehazenet: an end-to-end system for single image haze removal. IEEE Trans. Image Process. 25 (11), 5187–5198.
Choi, L.K., You, J., Bovik, A.C., 2015. Referenceless prediction of perceptual fog density and perceptual image defogging. IEEE Trans. Image Process. 24 (11), 3888–3901.
Fang, Y., Ma, K., Wang, Z., Lin, W., Fang, Z., Zhai, G., 2015. No-reference quality assessment of contrast-distorted images based on natural scene statistics. IEEE Signal Process. Lett. 22 (7), 838–842.
Fattal, R., 2008. Single image dehazing. ACM Trans. Graphics 27 (3), 1–9.
Fattal, R., 2014. Dehazing using color-lines. ACM Trans. Graphics 34 (1), 1–14.
He, K., Sun, J., Tang, X., 2010. Single image haze removal using dark channel prior. IEEE Trans. Pattern Anal. Mach. Intell. 33 (12), 2341.
Kolmogorov, V., Zabih, R., 2004. What energy functions can be minimizedvia graph cuts? IEEE Trans. Pattern Anal. Mach. Intell. 26 (2), 147–159.
Kopf, J., Neubert, B., Chen, B., Cohen, M., Cohen-Or, D., Deussen, O., Uyttendaele, M., Lischinski, D., 2008. Deep photo: model-based photograph enhancement and viewing. Proc. ACM SIGGRAPH Asia. pp. 116.
Li, Y., You, S., Brown, M.S., Tan, R.T., 2016. Haze visibility enhancement: a survey and quantitative benchmarking. arXiv preprintarXiv:1607.06235.
Li, Z., Zheng, J., 2015. Edge-preserving decomposition based single image haze removal. IEEE Trans. Image Process. 24 (12), 5432.
Ma, K., Duanmu, Z., Wu, Q., Wang, Z., Yong, H., Li, H., Zhang, L., 2016. Waterloo exploration database: new challenges for image quality assessment models. IEEE Trans. Image Process. 26 (2), 1004–1016.
Martin, D., Fowlkes, C., Tal, D., Malik, J., 2001. A database of human segmented natural images and its application to evaluating segmentation algorithms and measuring ecological statistics. Proc. ICCV. Vol. 2. pp. 416–423.
Meng, G., Wang, Y., Duan, J., Xiang, S., Pan, C., 2013. Efficient image dehazing with boundary constraint and contextual regularization. Proc. ICCV. pp. 617–624.
Middleton, W.E.K., 1954. Vision through the atmosphere. Phys. Today 7 (3). 21–21
Narasimhan, S.G., Nayar, S.K., 2000. Chromatic framework for vision in bad weather. Proc. CVPR. pp. 598–605.
Nishino, K., Kratz, L., Lombardi, S., 2012. Bayesian defogging. Int. J. Comput. Vis. 98 (3), 263–278.
Park, D., Han, D.K., Jeon, C., Ko, H., 2013. Fast single image de-hazing using characteristics of RGB channel of foggy image. Ieice Trans. Inf. Syst. E96.D (8), 1793–1799.
Schechner, Y.Y., Narasimhan, S.G., Nayar, S.K., 2001. Instant dehazing of images using polarization. Proc. CVPR. pp. 325.
Sulami, M., Glatzer, I., Fattal, R., Werman, M., 2014. Automatic recovery of the atmospheric light in hazy images. Proc. ICCP. pp. 1–11.
Tan, R.T., 2008. Visibility in bad weather from a single image. Proc. CVPR. pp. 1–8.
Tang, K., Yang, J., Wang, J., 2014. Investigating haze-relevant features in a learning framework for image dehazing. Proc. CVPR. pp. 2995–3002.
Tarel, J.P., Hautire, N., 2010. Fast visibility restoration from a single color or gray level image. Proc. ICCV. pp. 2201–2208.
Wang, S., Ma, K., Yeganeh, H., Wang, Z., Lin, W., 2015. A patch-structure representation method for quality assessment of contrast changed images. IEEE Signal Process. Lett. 22 (12), 2387–2390.
Wang, Z., Bovik, A.C., Sheikh, H.R., Simoncelli, E.P., 2004. Image quality assessment: from error visibility to structural similarity. IEEE Trans. Image Process. 13 (4), 600–612.
Zhu, Q., Mai, J., Shao, L., 2015. A fast single image haze removal algorithm using color attenuation prior. IEEE Trans. Image Process. 24 (11), 3522.